Cell

Coordinated Ciliary Beating Requires *Odf2*-Mediated Polarization of Basal Bodies via Basal Feet

Koshi Kunimoto,[1] Yuji Yamazaki,[1,8] Tomoki Nishida,[2,8] Kyosuke Shinohara,[3,8] Hiroaki Ishikawa,[4,8] Toshiaki Hasegawa,[2] Takeshi Okanoue,[5] Hiroshi Hamada,[3] Tetsuo Noda,[6] Atsushi Tamura,[1] Shoichiro Tsukita,[7] and Sachiko Tsukita[1,*]

[1]Laboratory of Biological Science, Graduate School of Frontier Biosciences and Graduate School of Medicine, Osaka University, Osaka 565-0871, Japan

[2]Research Center for Ultra-high Voltage Electron Microscopy, Osaka University, Osaka 567-0047, Japan

[3]Developmental Genetics Group, Graduate School of Frontier Biosciences, Osaka University and CREST, Japan Science and Technology Corporation (JST), Osaka 565-0871, Japan

[4]Department of Biochemistry and Biophysics, University of California, San Francisco, San Francisco, CA 94143, USA

[5]Department of Hepatology, Saiseikai Suita Hospital, Osaka 564-0013, Japan

[6]Department of Cell Biology, Cancer Institute of Japanese Foundation for Cancer Research, Tokyo 135-8550, Japan

[7]Department of Cell Biology, Faculty of Medicine, Kyoto University, Yoshida-Konoe, Kyoto 606-8315, Japan

[8]These authors contributed equally to this work

*Correspondence: atsukita@biosci.med.osaka-u.ac.jp

DOI 10.1016/j.cell.2011.10.052

SUMMARY

Coordinated beating of cilia in the trachea generates a directional flow of mucus required to clear the airways. Each cilium originates from a barrel-shaped basal body, from the side of which protrudes a structure known as the basal foot. We generated mice in which exons 6 and 7 of *Odf2*, encoding a basal body and centrosome-associated protein Odf2/cenexin, are disrupted. Although $Odf2^{\Delta Ex6,7/\Delta Ex6,7}$ mice form cilia, ciliary beating is uncoordinated, and the mice display a coughing/sneezing phenotype. Whereas residual expression of the C-terminal region of *Odf2* in these mice is sufficient for ciliogenesis, the resulting basal bodies lack basal feet. Loss of basal feet in ciliated epithelia disrupted the polarized organization of apical microtubule lattice without affecting planar cell polarity. The requirement for *Odf2* in basal foot formation, therefore, reveals a crucial role of this structure in the polarized alignment of basal bodies and coordinated ciliary beating.

INTRODUCTION

Multiciliary apical differentiation is primarily associated with airway epithelial, ependymal, and oviductal epithelial cells. The coordinated beating of cilia in multiciliary airway cells creates luminal flow, which plays critical roles in the directional diffusion of the apical mucus layer, which establishes respiratory defense mechanisms; defects in this directional diffusion cause primary ciliary dyskinesia, including chronic bronchiectasis, sinusitis, and otitis media (Afzelius, 1979; Badano et al., 2006; Morillas et al., 2007; Sloboda and Rosenbaum, 2007; Zariwala et al., 2007).

It has recently been proposed that planar cell polarity (PCP) plays a key role in the coordination of ciliary beating, in which PCP core proteins transduce chains of cell signaling along PCP pathways to organize PCP effector proteins, thereby regulating epithelial sheet orientation, and thus the direction of ciliary beating (Marshall, 2010; Marshall and Kintner, 2008; McNeill, 2010; Vladar and Axelrod, 2008; Wallingford, 2010; Zallen, 2007). The PCP core proteins include at least three surface proteins (Frizzled/Vangl/Celsr) and three cytoplasmic proteins (Dishevelled/Prickle/Inversin). Fuzzy and Inturned have been identified as PCP effector proteins, which may regulate the polarized arrangement of cilia in multiciliated cells downstream of the core proteins (Gray et al., 2009; Heydeck et al., 2009; Park et al., 2006, 2008). These effector proteins reportedly regulate polarization of basal bodies, from which the axoneme of the ciliary shafts extend; the molecular mechanism underlying this process, however, remains elusive.

A wealth of evidence suggests that the directionality of ciliary beating is determined by the orientation of basal bodies, which are regularly associated with basal feet at positions 4, 5, and 6 of circularly arranged triplets of microtubules of basal bodies (Anderson, 1972; Boisvieux-Ulrich et al., 1985; Gibbons, 1961; Reed et al., 1984; Sorokin, 1968). Microtubule doublets extend from each triplet to form a ciliary axoneme encircling a central pair of microtubules, collectively forming a ciliary shaft. The coordinated orientation of basal bodies due to PCP is thus required for the coordination of ciliary beating. On the other hand, basal bodies are also reportedly associated with cytoplasmic nonciliary microtubules through basal feet situated beneath the apical membrane, thus forming an apical microtubular lattice (Gordon, 1982; Hard and Rieder, 1983; Reed et al., 1984). Although it is thought that the basal feet play a critical role in polarization of the basal bodies and cilia, as well as in

the organization of the microtubular lattice in multiciliated cells, evidence for this at the molecular level is lacking.

The *Odf2* gene was initially identified as the gene that encodes one of the major components of outer dense fiber (ODF), which is a highly stable fibrous structure in the sperm tail (Brohmann et al., 1997; Oko and Clermont, 1988), and its gene product was later identified as an antigen of the antibody against centrosomal appendages (Nakagawa et al., 2001). The gene for the cenexin protein, which was first identified as a protein marker of the mother centriole (Lange and Gull, 1995), was subsequently found to be identical to *Odf2* and encodes transcripts cenexin 1 and cenexin 2 (NCBI submissions gi:8886474 and gi:17388905, respectively). It was later shown that *Odf2* is ubiquitously expressed in many cell types as various splicing variants (Schweizer and Hoyer-Fender, 2009; Soung et al., 2006, 2009). Here, we describe the gene products of *Odf2* gene under the protein name, Odf2/cenexin. *Odf2* has been reported to play a key role in the formation of primary cilia (Ishikawa et al., 2005; Soung et al., 2009) and sperm flagella (Tarnasky et al., 2010). In F9 cells, deletion of exons 7–10 of the 22 exons of *Odf2*, which correspond to exons 6–9 in the present study, resulted in a defect in the formation of the primary cilium, as well as in loss of the distal and subdistal appendages of the centriole (Ishikawa et al., 2005). A short primary cilia phenotype was observed in another cell line in which cenexin 1, encoded by a splice variant of *Odf2*, was knocked down (Soung et al., 2009).

To analyze the function of *Odf2*, we produced $Odf2^{\Delta Ex6,7/\Delta Ex6,7}$ mice in which exons 6 and 7 of *Odf2* were genetically disrupted, with the aim of generating a null allele. Because of the infertility of $Odf2^{flox\text{-}del/+}$ male mice, we mated the $CAG^{cre/+};Odf2^{flox\text{-}del/+}$ female mice with $Odf2^{flox/+}$ male mice to generate *Odf2*-exon 6,7-disrupted mice, which showed coughing- and sneezing-like phenotypes due to primary ciliary dyskinesia (Sternberg et al., 1981). In contrast to $Odf2^{-/-}$ F9 cells (Ishikawa et al., 2005), the mice form cilia but exhibit defects in coordinated multiciliary beating, as shown in $Odf2^{\Delta Ex6,7/\Delta Ex6,7}$ trachea. Further analysis revealed that a C-terminal portion of *Odf2* is expressed in $Odf2^{\Delta Ex6,7/\Delta Ex6,7}$ mice, and transfection of this domain into $Odf2^{-/-}$ F9 cells rescues cilia formation, suggesting that the C-terminal region of *Odf2* is sufficient for cilia formation. However, cilia in $Odf2^{\Delta Ex6,7/\Delta Ex6,7}$ mice exhibit a striking loss of basal feet, poorly understood structures that connect to 4,5,6-numbered triplets of basal bodies, and are also regularly associated with the cytoplasmic microtubules, but the role of which is unknown. The present study for the first time reveals that *Odf2* is indispensable for the formation of basal feet in vivo. Our findings further indicate that basal feet play a critical role in PCP-dependent organization of the apical microtubular lattice and PCP-based arrangement of basal bodies that underlie coordinated multiciliary beating.

RESULTS

$Odf2^{\Delta Ex6,7/\Delta Ex6,7}$ Mice Display Primary Ciliary Dyskinesia

Because $Odf2^{flox\text{-}del/+}$ male mice were infertile (as confirmed in > 10 males), female $CAG^{cre/+};Odf2^{flox\text{-}del/+}$ mice were intercrossed with male $Odf2^{flox/+}$ mice to obtain $Odf2^{\Delta Ex6,7/\Delta Ex6,7}$ mice (Figure 1 and see Figures S1A and S1B available online). $Odf2^{\Delta Ex6,7/\Delta Ex6,7}$ mice were born at a Mendelian ratio, and characterized by lower body weight, ~70%–80% that of $Odf2^{+/+}$ littermates (Figures 2A, S1C, and S1D). The survival rate of $Odf2^{\Delta Ex6,7/\Delta Ex6,7}$ mice gradually decreased after birth, with only 20% surviving beyond weaning (Figure S1E).

The surviving $Odf2^{\Delta Ex6,7/\Delta Ex6,7}$ mice were characterized by a coughing/sneezing-like phenotype (maximum 13.3 Hz), as evaluated by sound waveform analysis (Figure 2B and Movie S1). However, increased levels of inflammation were not observed in the $Odf2^{\Delta Ex6,7/\Delta Ex6,7}$ mice lung, as revealed by hematoxylin and eosin staining (H&E) of lung preparations (Figure S1F), which we suggest is at least in part due to the specific pathogen-free (SPF) conditions. The $Odf2^{\Delta Ex6,7/\Delta Ex6,7}$ mice were also characterized by sinusitis and otitis media ($Odf2^{+/+}$: n = 4, bilateral negative; $Odf2^{\Delta Ex6,7/\Delta Ex6,7}$: n = 4, bilateral positive) (Figures 2C and 2D), suggesting that *Odf2* deficiency causes primary ciliary dyskinesia in mice. In addition we detected a slight tendency to hydrocephaly (three $Odf2^{+/+}$ and $Odf2^{\Delta Ex6,7/\Delta Ex6,7}$ pairs examined) on detailed examination of H&E preparations ($Odf2^{+/+}$: negative [n = 3]; $Odf2^{\Delta Ex6,7/\Delta Ex6,7}$: negative [n = 1], mild positive [n = 2]) (Figure S1G). These defects were not causes of death among the more than 100 $Odf2^{\Delta Ex6,7/\Delta Ex6,7}$ mice evaluated, although the early postnatal death of $Odf2^{\Delta Ex6,7/\Delta Ex6,7}$ mice is likely attributable to impaired gastrointestinal motility, possibly caused by the coincident development of Hirschsprung's disease.

$Odf2^{\Delta Ex6,7/\Delta Ex6,7}$ mice were expected to show a lethal phenotype, possibly due to the loss of primary cilia in somatic cells as suggested by the loss of cilia phenotype in $Odf2^{-/-}$ F9 cells (Ishikawa et al., 2005). However, surprisingly, $Odf2^{\Delta Ex6,7/\Delta Ex6,7}$ mice were born with primary cilia. We examined the protein expression of Odf2/cenexin and expression of *Odf2* mRNA in various organs of $Odf2^{\Delta Ex6,7/\Delta Ex6,7}$ mice (Figures 1C and 1D). First, we examined the protein expression of Odf2/cenexin by western blotting. We did not detect full-length *Odf2* gene products around 90 kDa or their fragments in the $Odf2^{\Delta Ex6,7/\Delta Ex6,7}$ tissues using two rabbit polyclonal antibodies, designated here as Odf2-N1 pAb and Odf2-N2 pAb. Odf2-N1 and Odf2-N2 pAbs were derived from the different antigens of the N-terminal regions of Odf2/cenexin at the 44–158 and 67–292 aa regions, respectively, of ENSEMBL accession number ENSMUST 00000028128 clone (Figure 1C and data not shown).

However, using an antibody raised against the C-terminal region of Odf2/cenexin, we detected slight immunofluorescence signals at the bases of cilia in $Odf2^{\Delta Ex6,7/\Delta Ex6,7}$ multiciliated tracheal cells, but not in $Odf2^{-/-}$ F9 cells (Figure S1H). Because exons 6 and 7, which encode the N-terminal region of *Odf2*, were deleted in the knockout strategy of *Odf2* in this study, we examined the expression of *Odf2* mRNA, probed with 3′ probes for the C-terminal region of the protein. mRNA corresponding to the *Odf2* C-terminal fragment was detected, albeit at 10%–30% of the level of wild-type *Odf2* mRNA, in numerous organs (Figure 1D). These results contrasted with those of $Odf2^{-/-}$ F9 cells in which a different targeting vector construct from that in $Odf2^{\Delta Ex6,7/\Delta Ex6,7}$ mice was integrated, and the expression of *Odf2* mRNAs was nearly completely suppressed to ~1.2% of

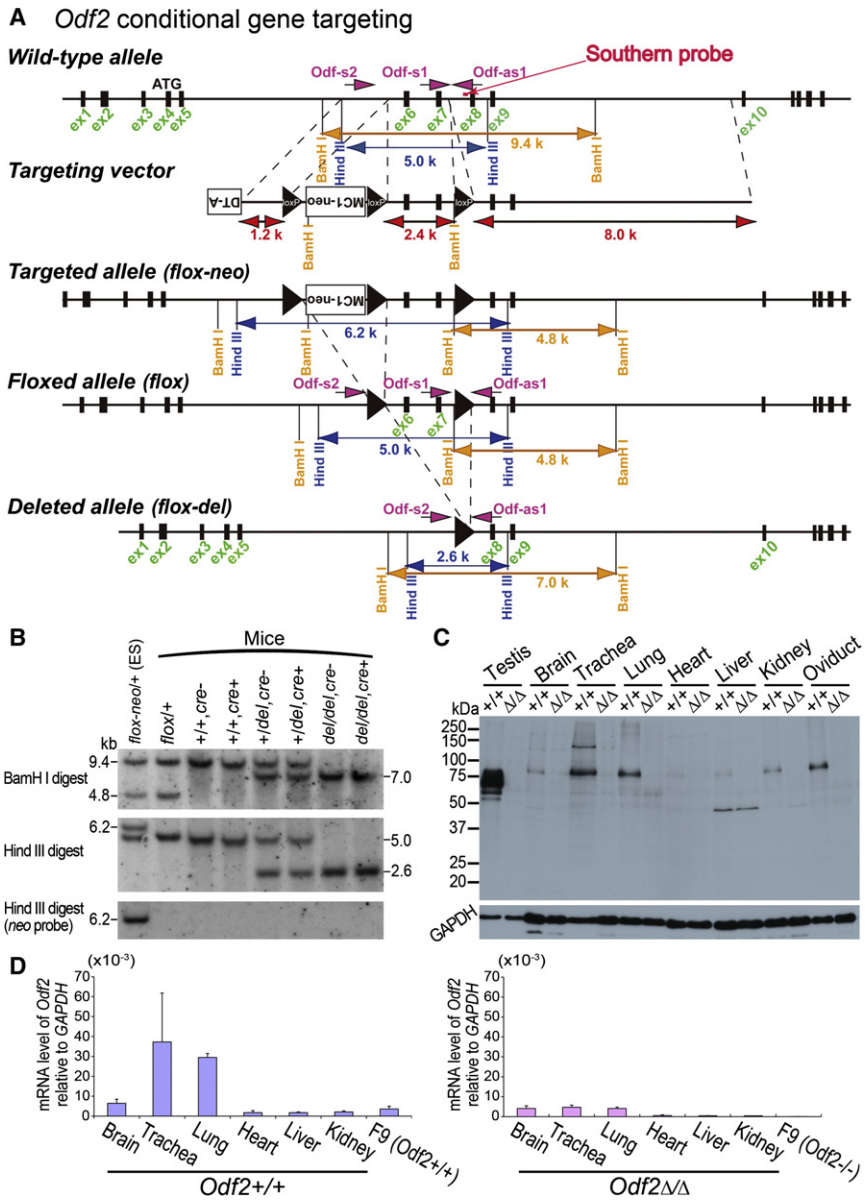

Figure 1. Generation of *Odf2*-Deficient Mice

(A) Construction of the wild-type allele, targeting vector, targeted allele, floxed allele, and deleted allele of the mouse *Odf2* gene. The targeting vector contained the *neo* cassette for selection, and *loxP* fragments (►) were located on both sides of exons 6 and 7 to delete these exons in the targeted allele (exon information from the ENSEMBL accession number: ENSMUST00000046571 clone).

(B) Genotype analyses of $Odf2^{\Delta Ex6,7/\Delta Ex6,7}$ mice. Southern blots of BamHI- or Hind III-digested genomic DNA from mice bearing the wild-type (+/+), heterozygous (+/ΔEx6,7: described here as +/del), or homozygous (ΔEx6,7/ΔEx6,7: described here as del/del) *Odf2* allele. The Cre recombinase activity was from Cre protein, its mRNA, or both, which were maintained in mature oocytes.

(C) Immunoblotting of mouse tissue samples by rabbit anti-Odf2/cenexin pAb, which reacts with the N-terminal region of Odf2/cenexin. The amount of testis sample protein loaded was one-tenth that of the other tissue samples. Specific bands for Odf2/cenexin were detected at about 90 kDa, except for testis, in which it was 75 kDa because of the lack of C-terminal extension of Odf2/cenexin; these bands specifically disappeared in the $Odf2^{\Delta Ex6,7/\Delta Ex6,7}$ tissues. Note that no specific expression of fragments derived from the Odf2/cenexin proteins was detected in the $Odf2^{\Delta Ex6,7/\Delta Ex6,7}$ tissues compared with $Odf2^{+/+}$, as revealed by Odf2-N1 pAb.

(D) Real-time RT-PCR analysis of the C-terminal region of *Odf2* in mouse tissues and F9 cells. Real-time RT-PCR analysis was performed for C-terminal *Odf2* in $Odf2^{+/+}$ and $Odf2^{\Delta Ex6,7/\Delta Ex6,7}$ tissues and $Odf2^{+/+}$ and $Odf2^{-/-}$ F9 cells, by an *Odf2*-3′ probe. The amount of *Odf2* mRNA was substantially or severely downregulated in the $Odf2^{\Delta Ex6,7/\Delta Ex6,7}$ mouse tissues or $Odf2^{-/-}$ F9 cells, respectively, compared with the $Odf2^{+/+}$ tissues and $Odf2^{+/+}$ F9 cells. The ratio of mRNA relative to *GAPDH* mRNA is indicated on the y axis. Error bars indicate SD (n = 3 except for $Odf2^{\Delta Ex6,7/\Delta Ex6,7}$ tissues [n = 2]).

See also Figure S1.

that in the $Odf2^{+/+}$ F9 cells. The unexpected viability and ciliogenesis of $Odf2^{\Delta Ex6,7/\Delta Ex6,7}$ mice is, therefore, likely attributable to the differences in expression of C-terminal *Odf2* mRNA between $Odf2^{\Delta Ex6,7/\Delta Ex6,7}$ mice and $Odf2^{-/-}$ F9 cells (Figure 1D and also see Figure 3D).

Basal Bodies Are Associated with Apical Membranes of $Odf2^{\Delta Ex6,7/\Delta Ex6,7}$ Multiciliated Epithelial Cells

Because the coughing/sneezing-like phenotype was prominent in $Odf2^{\Delta Ex6,7/\Delta Ex6,7}$ mice, we examined the localization of Odf2/cenexin in $Odf2^{+/+}$ and $Odf2^{\Delta Ex6,7/\Delta Ex6,7}$ ciliated epithelial cells in the trachea using Odf2-N2 pAb. Immunofluorescence labeling using an antibody that detects an N-terminal epitope of Odf2/cenexin revealed labeling of the bases of cilia in tracheal multiciliated cells in $Odf2^{+/+}$ mice. In contrast in $Odf2^{\Delta Ex6,7/\Delta Ex6,7}$ mice, the Odf2/cenexin signal almost disappeared, although cilia in tracheal multiciliated cells were present, as shown by immunofluorescence for acetylated α-tubulin (Figure 3A). Scanning electron microscopy, which clearly distinguished individual ciliated cells and cilia, demonstrated that the number of ciliated cells was not different in the $Odf2^{+/+}$ and $Odf2^{\Delta Ex6,7/\Delta Ex6,7}$ tracheas, although the number of cilia per single multiciliated tracheal cell was lower in $Odf2^{\Delta Ex6,7/\Delta Ex6,7}$ tracheal multiciliated cells than in $Odf2^{+/+}$ cells (Figures S2A–S2C). Notably, there was no difference in the lengths of cilia in multiciliated cells, as shown by scanning electron microscopy (Figure S2D).

We also confirmed by immunofluorescence the same tendency toward a decrease in the number of cilia per cell in $Odf2^{\Delta Ex6,7/\Delta Ex6,7}$ multiciliated cells of the oviduct and ventricle in brain (Figure S2E). Immunofluorescence for γ-tubulin, as

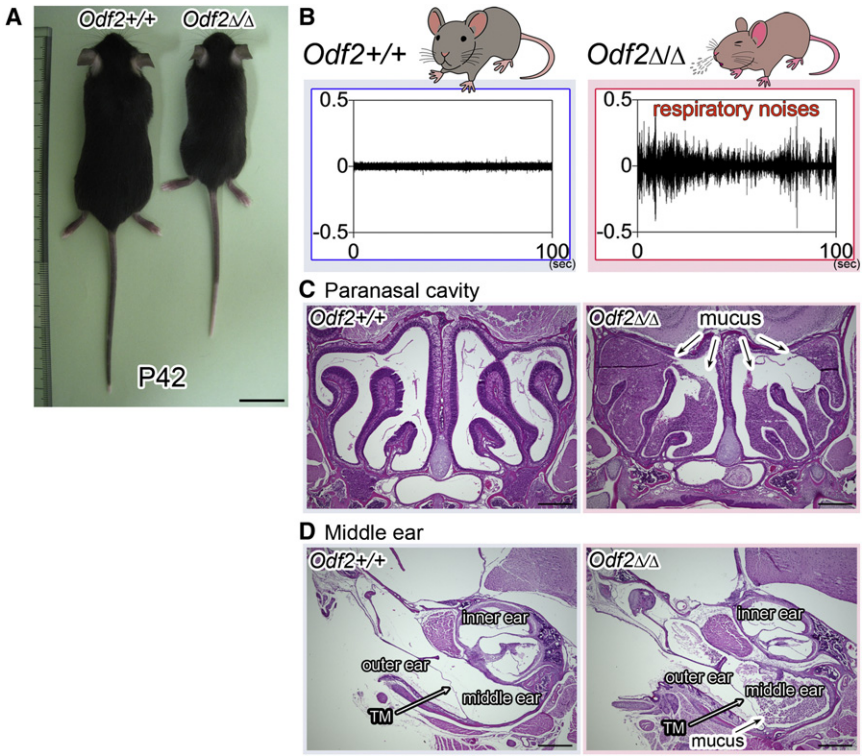

Figure 2. Primary Ciliary Dyskinesia in *Odf2*$^{\Delta Ex6,7/\Delta Ex6,7}$ Adult Mice

(A) P42 *Odf2*$^{+/+}$ and *Odf2*$^{\Delta Ex6,7/\Delta Ex6,7}$ littermates. Scale bar, 2 cm.

(B) Coughing/sneezing-like phenotype of the *Odf2*$^{\Delta Ex6,7/\Delta Ex6,7}$ mice. Analysis of mouse respiratory sounds.

(C) H&E of the paranasal cavity with sinusitis. Massive amounts of mucus were observed in the *Odf2*$^{\Delta Ex6,7/\Delta Ex6,7}$ bilateral paranasal cavity. Scale bars, 0.5 mm.

(D) H&E of the middle ear. Accumulated mucus was observed in the *Odf2*$^{\Delta Ex6,7/\Delta Ex6,7}$ middle ear, consistent with otitis media. The tympanic membranes (TM) are indicated by a white arrow. Scale bars, 0.5 mm.

See also Figure S1 and Movie S1.

a marker for basal bodies (Lüders and Stearns, 2007; Vladar and Stearns, 2007), as well as ultra-high-voltage electron microscopic tomography (UHVEMT) of sagittal sections of tracheal cells revealed that the *Odf2*$^{\Delta Ex6,7/\Delta Ex6,7}$ cilium nucleates from the basal body, as is the case for the wild-type *Odf2*$^{+/+}$ cilium (Figures 3B and 3C and Movie S2). However, some *Odf2*$^{\Delta Ex6,7/\Delta Ex6,7}$ basal bodies fail to position apically, suggesting a partial disorder in the transport and/or docking of basal bodies to the apical membrane (Gray et al., 2009; Park et al., 2008; Vladar and Axelrod, 2008; Voronina et al., 2009).

When we examined *Odf2*$^{\Delta Ex6,7/\Delta Ex6,7}$ primary cilia, we found that acetylated α-tubulin-positive primary cilia were present in *Odf2*$^{\Delta Ex6,7/\Delta Ex6,7}$ tissues, just as in *Odf2*$^{+/+}$ mice, although the lengths of primary cilia were significantly decreased, shortened by ~30% compared with the average length of *Odf2*$^{+/+}$primary cilia (see Figures S3A and S3B). These findings were consistent with the short primary cilia phenotype in HeLa cells in which *Odf2* is knocked down (Soung et al., 2009) but not consistent with the lack of cilia phenotype in *Odf2*$^{-/-}$ F9 cells (Ishikawa et al., 2005).

Given the expression of C-terminal region of *Odf2* mRNA in *Odf2*$^{\Delta Ex6,7/\Delta Ex6,7}$ mice, but not in *Odf2*$^{-/-}$ F9 cells, we exogenously expressed the C-terminal region of *Odf2* in *Odf2*$^{-/-}$ F9 cells (Figure 3D). Among the GFP-tagged constructs of the C-terminal region, as well as full-length and N-terminal constructs, we found that the primary cilia were significantly generated from the basal bodies by transfection of full-length and C-terminal *Odf2*-constructs, as revealed in immunofluorescence microscopy, although N-terminal constructs and short C-terminal constructs had no effect on generation of primary cilia (Figure 3D). Generation of primary cilia in *Odf2*$^{\Delta Ex6,7/\Delta Ex6,7}$ mice is, therefore, likely to be a result of the expression of C-terminal sequences of *Odf2* mRNA.

Disruption of Coordinated Movement of Cilia and Mucociliary Transport

These findings in *Odf2*$^{\Delta Ex6,7/\Delta Ex6,7}$ mice prompted us to examine multiciliary beating in live cells. Live imaging of isolated trachea preparations by high-speed imaging (500 frames/s) allowed us to analyze the behavior of tracheal cilia on the tracheal luminal surface. In the *Odf2*$^{+/+}$ trachea preparation, every cilium beats in the typical manner, generating metachronal waves in an adoral direction, replicating their orientation in vivo (Figure 4A and Movie S3). In contrast in the *Odf2*$^{\Delta Ex6,7/\Delta Ex6,7}$ trachea preparation, this coordinated ciliary beating was apparently perturbed between tufts (coordinated groups of cilia) and/or shafts (extracellular protrusions of a cilium). Circular plot analyses in which the lung-to-oral direction was set at 225°–45° revealed ciliary beating that was nearly uniformly oriented in the lung-to-oral direction in *Odf2*$^{+/+}$ wild-type trachea but highly dispersed in *Odf2*$^{\Delta Ex6,7/\Delta Ex6,7}$ mutant trachea (Figure 4A and Movie S3). Thus, the coordination of multiciliary beating was affected by deficiency of full-length *Odf2*.

We next examined the effects of the deficiency of full-length *Odf2* on mucociliary transport in the tracheal lumen. Using live imaging, we monitored fluid flow across the luminal surface of the trachea by adding fluorescent beads to the medium and making time-lapse movies of bead movements; as described above, the lung-to-oral direction was set arbitrarily at 225°–45° in our analyses (Figures 4B and 4C and Movie S3). In wild-type *Odf2*$^{+/+}$ tracheas the fluorescent beads flowed in a lung-to-oral direction, suggesting that the in vivo situation was at least partly reproduced. In sharp contrast in the mutant *Odf2*$^{\Delta Ex6,7/\Delta Ex6,7}$ trachea, the fluorescent beads did not exhibit overall unidirectional flow, showing only limited, uncoordinated movement. The velocity of bead movement in *Odf2*$^{+/+}$ trachea appeared to be higher than that in *Odf2*$^{\Delta Ex6,7/\Delta Ex6,7}$ trachea. These findings indicate that the deficiency of exons 6 and 7 of *Odf2* blocks

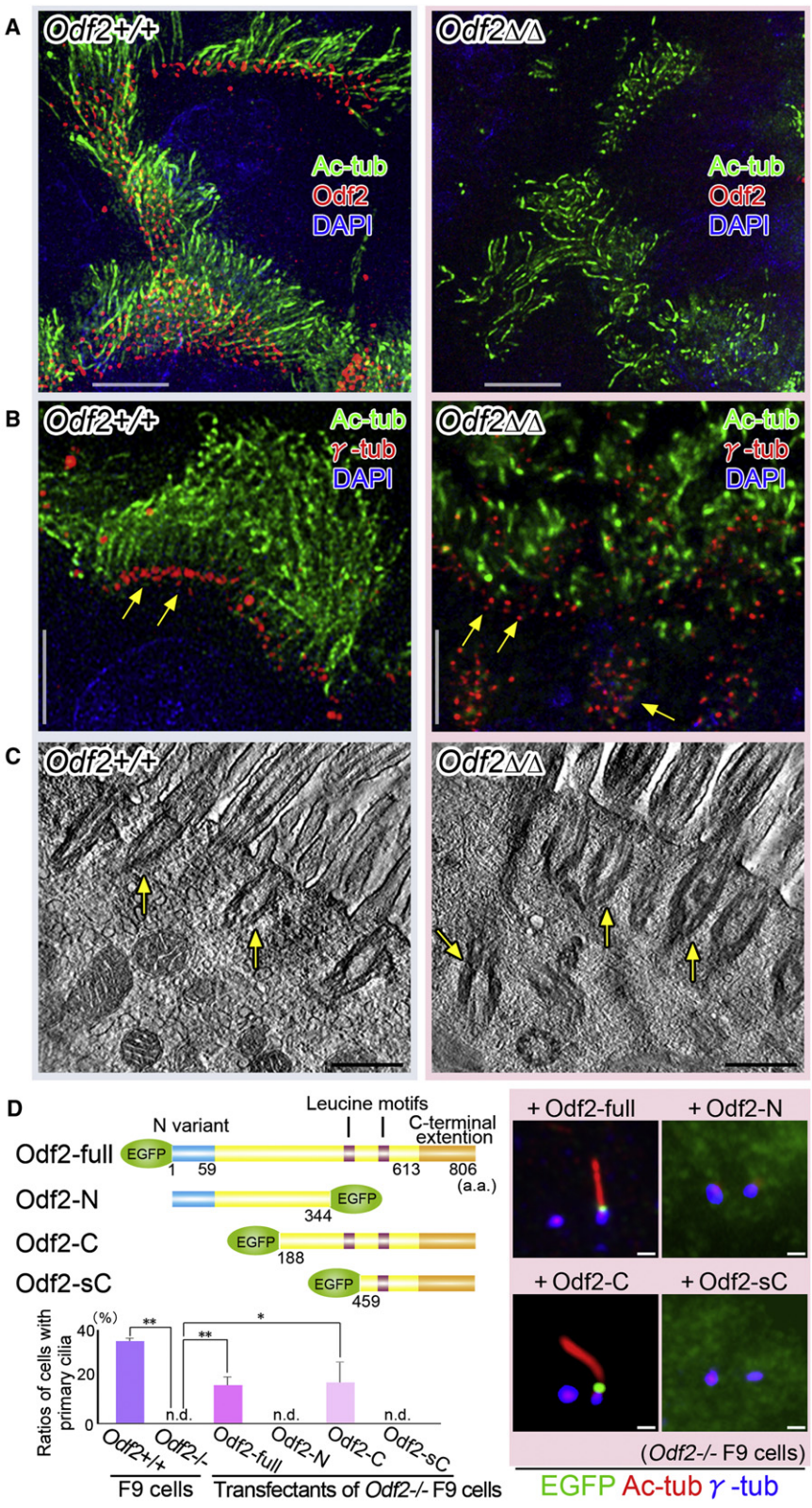

Figure 3. Disordered Arrangement of Cilia in *Odf2*$^{\Delta Ex6,7/\Delta Ex6,7}$ Adult Mice and Dependency of C-Terminal Region of *Odf2* on Ciliogenesis

(A) Immunofluorescence micrographs of *Odf2*$^{+/+}$ and *Odf2*$^{\Delta Ex6,7/\Delta Ex6,7}$ ciliated tracheal epithelial cells. Ac-tub, acetylated α-tubulin (green); Odf2, Odf2/cenexin (red); DAPI (blue). Scale bars, 5 μm.

(B) Immunofluorescence micrographs of *Odf2*$^{+/+}$ and *Odf2*$^{\Delta Ex6,7/\Delta Ex6,7}$ ciliated tracheal epithelial cells. Ac-tub, acetylated α-tubulin (green); γ-tub, γ-tubulin (red); DAPI (blue). Yellow arrows indicate γ-tubulin-positive basal bodies. Scale bars, 5 μm.

(C) Selected tomographic slices of UHVEMT of the tracheal ciliated cells in the sagittal view (see Movie S2). Yellow arrows indicate basal bodies. Scale bars, 0.5 μm.

(D) Immunofluorescence micrographs of primary cilia in *Odf2*$^{-/-}$ F9 cells transfected by full-length or deleted mutants of *Odf2*, in which the generation of primary cilia was completely suppressed. The schematic drawing shows GFP-tagged constructions of *Odf2*. Odf2-full: the gene product of GFP-tagged full-length of *Odf2* (ENSMUST00000113757). Odf2-N, Odf2-C, and Odf2-sC: the gene products of GFP-tagged N-terminal, C-terminal, and short C-terminal region of *Odf2*, respectively. The right-upper panel shows the generation of primary cilia in cells transfected with *Odf2*-full and *Odf2*-C. EGFP (green); Ac-tub, acetylated α-tubulin (red); γ-tub, γ-tubulin (blue). Scale bars, 0.5 μm. Graph of the ratio of cells containing primary cilia. In the *Odf2*$^{+/+}$ F9 cells, ~35% of F9 cells generated primary cilia. The complete loss of primary cilia in *Odf2*$^{-/-}$ F9 cells was restored by the exogenous expression of full-length *Odf2* (*Odf2*-full) and C-terminal domain of *Odf2* (*Odf2*-C) in ~20% of transfected cells. The percentage of primary cilia/centrosomes was calculated in each independent area. The experiments were independently repeated four times. Error bar, SEM. n.d., not detected. $^{**}p < 0.01$; $^{*}p < 0.05$.

See also Figures S1–S3 and Movie S2.

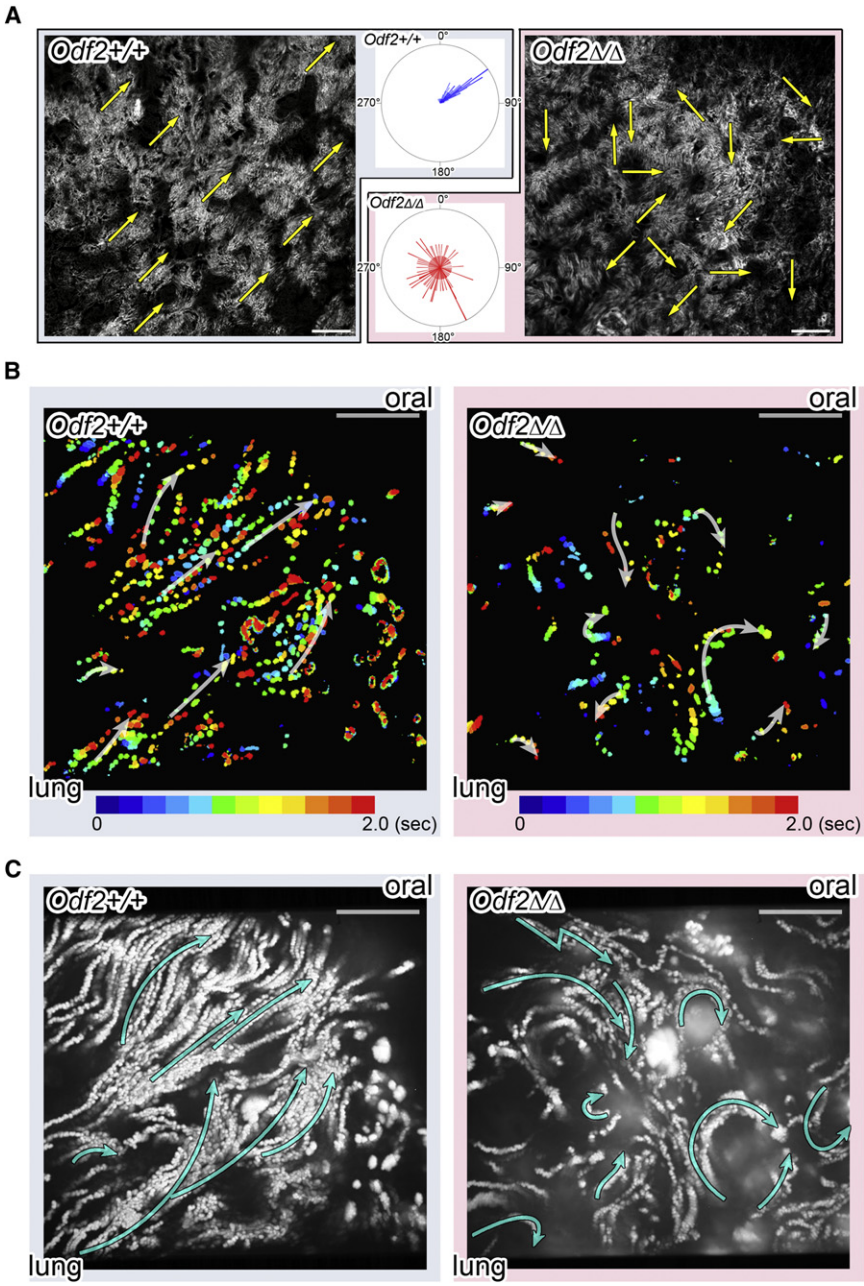

Figure 4. Aberrant Multiciliary Beating and Stagnant Mucociliary Transport in the *Odf2*$^{\Delta Ex6,7/\Delta Ex6,7}$ Trachea

(A) The image shows an enhanced view of cilia taken from Movie S3. Yellow arrows indicate direction of ciliary beating in multiciliated cells. The statistical analysis of beating directions is shown in the circular plots. *Odf2*$^{+/+}$, n = 202; *Odf2*$^{\Delta Ex6,7/\Delta Ex6,7}$, n = 224. Scale bars, 10 μm.

(B) Analysis of mucociliary transport velocity over tracheal explants for 2 s, measured by tracking fluorescent beads. The bead position at each time point is indicated in color, matching the scale at bottom. White arrows indicate direction of flow (the length represents relative migration lengths of beads for 1 s). Scale bars, 100 μm.

(C) Stacked images of the fluorescent bead traces, acquired over a 10 s interval (see Movie S3). Note that the coordinated mucociliary transport from the lung to the oral side is clear in the wild-type trachea but was stagnant in the *Odf2*$^{\Delta Ex6,7/\Delta Ex6,7}$ trachea. Cyan arrows indicate direction of flow (the length represents relative migration lengths of beads for 10 s). Scale bars, 100 μm.

See also Figure S2 and Movie S3.

effective directional mucociliary transport in trachea, which may cause the coughing/sneezing-like phenotype, in which forced expulsion of air serves to suppress infections in *Odf2*$^{\Delta Ex6,7/\Delta Ex6,7}$ mice. The bilateral sinusitis and otitis media observed in the mutant animals may be secondary to the inhibition of mucociliary transport in the paranasal sinus and middle ear (Figures 2C and 2D). *Odf2*$^{\Delta Ex6,7/\Delta Ex6,7}$ mice may, therefore, serve as a useful model of primary ciliary dyskinesia.

Depletion of Basal Feet in *Odf2*$^{\Delta Ex6,7/\Delta Ex6,7}$ Mice

It has been reported that disturbances in basal body polarization, as implicated by the relative positioning of basal feet, impair coordinated multiciliary beating and organization of luminal directed flow (Park et al., 2008). We stereoscopically examined the arrangement of basal bodies/basal feet just beneath the apical membranes in *Odf2*$^{+/+}$ and *Odf2*$^{\Delta Ex6,7/\Delta Ex6,7}$ mouse tracheal epithelial cells using UHVEMT. When basal bodies were closely examined by UHVEMT in cross-section, the typical 9+0 arrangement of microtubular triplets was discerned in both *Odf2*$^{+/+}$ and *Odf2*$^{\Delta Ex6,7/\Delta Ex6,7}$ mutant basal bodies. However, the regular distribution of basal bodies on the apical plane was disturbed in the *Odf2*$^{\Delta Ex6,7/\Delta Ex6,7}$ tracheal cell (Figure 5A). When we examined the basal foot, which is regularly associated with a distinct side of the basal body in *Odf2*$^{+/+}$ trachea, we found that the basal foot was completely lost in *Odf2*$^{\Delta Ex6,7/\Delta Ex6,7}$ tracheal epithelial cells.

We next closely examined the structures of each basal body by UHVEMT (Figure 5B and Movies S4 and S5), and clearly visualized the fine structure of basal bodies in *Odf2*$^{+/+}$ trachea in three dimensions. In the border region between the basal body and the ciliary shaft, the anchoring fibers were associated in a pinwheel pattern. At a position 160 nm distant from the anchoring fibers along the *Odf2*$^{+/+}$ basal body, the basal foot was associated with the basal body as a cone-like structure, 170 nm wide and 200 nm high, in which V-shaped plate-like structures divide the inner cone space into three

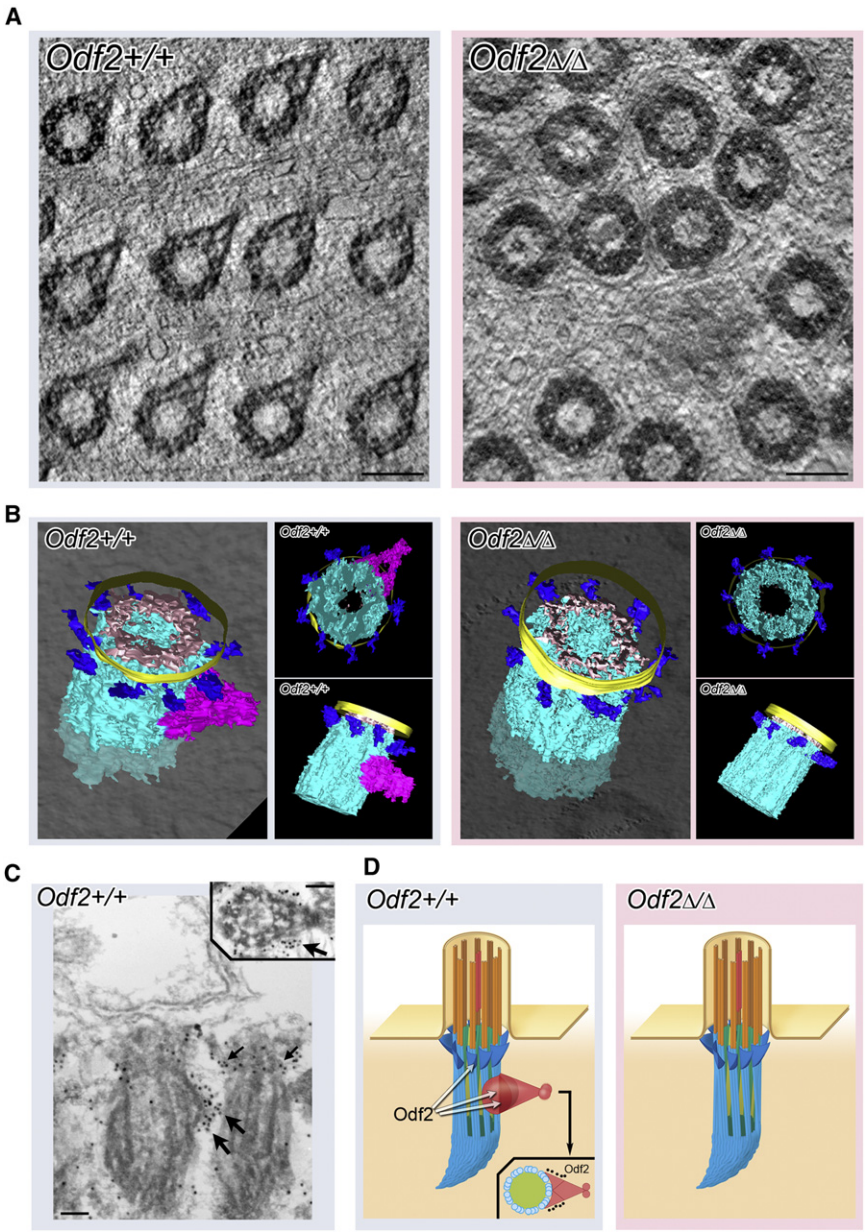

Figure 5. Loss of Basal Feet from the Basal Bodies in *Odf2*$^{\Delta Ex6,7/\Delta Ex6,7}$ Multiciliated Tracheal Cells

(A) Selected tomographic slices of UHVEMT of *Odf2*$^{+/+}$ and *Odf2*$^{\Delta Ex6,7/\Delta Ex6,7}$ tracheal epithelial cells at the level of the tips of the basal feet are shown (see Movies S4 and S5). Note that the regular arrangement of the basal bodies was disturbed in the *Odf2*$^{\Delta Ex6,7/\Delta Ex6,7}$ tracheal epithelial cells and that the basal feet (the cone shape at left) were missing. Scale bars, 0.2 μm.

(B) 3D reconstruction of basal bodies. Light blue indicates the main part of the basal body, pink shows basal foot, dark blue illustrates anchoring fibers, yellow indicates ciliary membrane, and whitish-pink structures show 9+0 arrangements of ciliary microtubules.

(C) Immunoelectron microscopic labeling for Odf2/cenexin by Odf2-N2 pAb in *Odf2*$^{+/+}$ basal bodies. Large arrows indicate immunogold signals on the basal feet. Small arrows show immunogold signals on anchoring fibers. Inset is a cross-sectional view of basal bodies at the level of the basal feet. Scale bar, 0.1 μm.

(D) Schematic drawings of *Odf2*$^{+/+}$ and *Odf2*$^{\Delta Ex6,7/\Delta Ex6,7}$ basal bodies. White arrows indicate Odf2-positive areas. Inset is a cross-sectional view of a basal body at the level of the basal foot.

See also Figures S3 and S4 and Movies S4–S7.

compartments (Figures 5A, 5B, and 5D and Movie S4). The base of the basal foot was associated with three triplet sets of microtubules, as an extension of ciliary microtubule doublets (numbers 4, 5, and 6) (Gibbons, 1961; Sorokin, 1968). The complete loss of the basal foot on deficiency of full-length *Odf2* was confirmed in 3D reconstructed images by UHVEMT (Figure 5B and Movies S4 and S5).

In other multiciliated cells, including oviductal epithelial cells and ependymal cells in brain, the basal feet are also absent in *Odf2*$^{\Delta Ex6,7/\Delta Ex6,7}$ mice, suggesting that the loss of basal feet may be a general phenomenon of *Odf2*$^{\Delta Ex6,7/\Delta Ex6,7}$ basal bodies (Figures S3C and S3D and Movie S6). When we examined the localization of Odf2/cenexin in the basal feet using immunoelectron microscopy, we found that Odf2/cenexin showed specific localization to the basal feet and the anchoring fibers (Figures 5C, 5D, and S4A–S4C). Although deletion of exon 6 and 7 of *Odf2* resulted in loss of basal feet, anchoring fibers remain attached to the basal bodies (Figures 5B and 5D). Taken together, our results show that *Odf2* is indispensable for basal foot formation.

In *Odf2*$^{-/-}$ F9 cells, another prominent phenotype in addition to the absence of cilia is loss of centrosomal subdistal appendages. The basal feet are generally regarded as modified centriolar subdistal appendages that project laterally from the sides of the triplet microtubule barrel (Anderson, 1972; Bornens, 2002; Seeley and Nachury, 2010). On immunofluorescence the signal for ninein at the subdistal appendage of the mother centriole was lost in the *Odf2*$^{\Delta Ex6,7/\Delta Ex6,7}$ mouse embryonic fibroblasts (MEFs) (Figure S5A). Hence, we examined the subdistal appendages of centrosomes in the *Odf2*$^{\Delta Ex6,7/\Delta Ex6,7}$ MEFs by UHVEMT (Figures S5B and S5C and Movie S7). Subdistal appendages, which radiated from the centrosomes in *Odf2*$^{+/+}$ MEFs, were absent in *Odf2*$^{\Delta Ex6,7/\Delta Ex6,7}$ MEFs, suggesting that the basal foot may be analogous to the centriolar subdistal appendage at the molecular level.

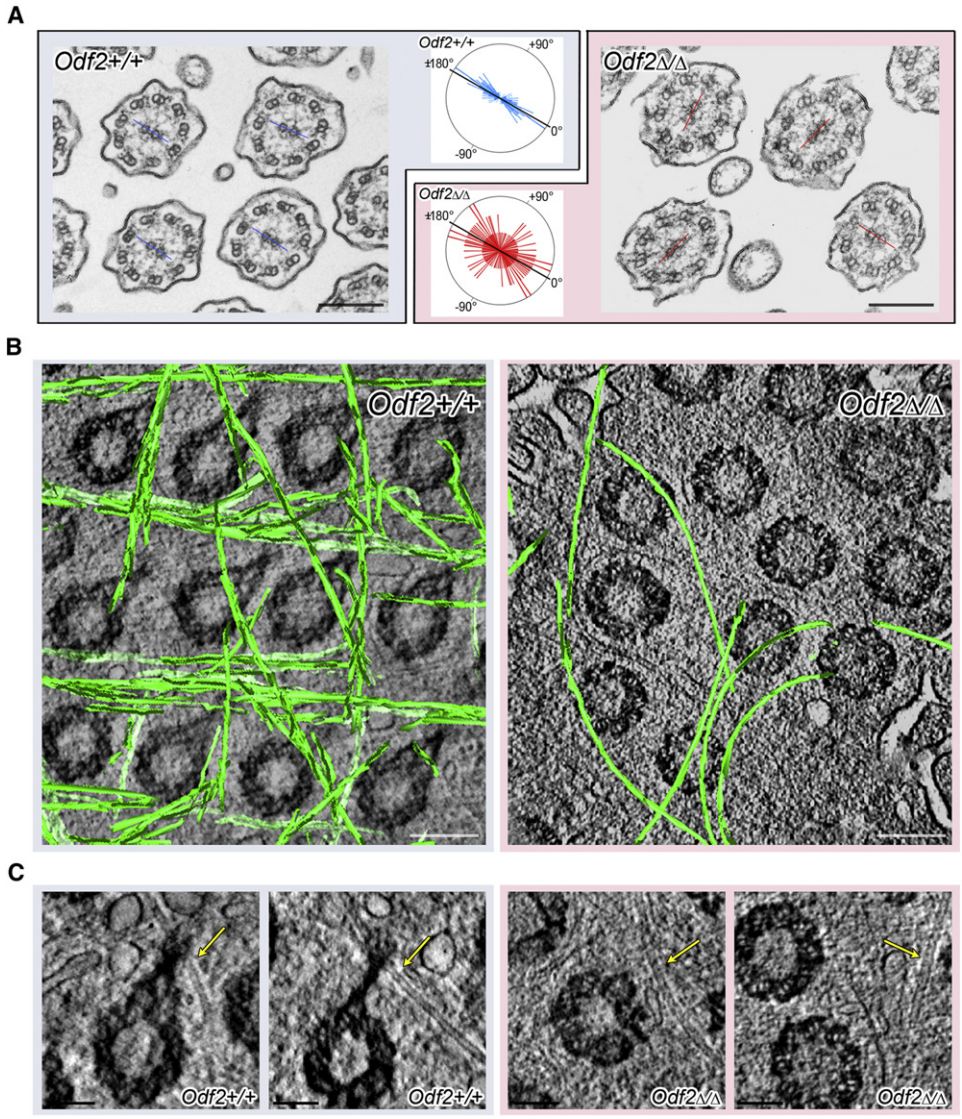

Figure 6. Rotational Polarity of Ciliary Axoneme and the Apical Microtubule Lattice in *Odf2*$^{+/+}$ and *Odf2*$^{\Delta Ex6,7/\Delta Ex6,7}$ Trachea

(A) Thin-section images of ciliary axonemes in the mouse trachea. The rotational polarity of each axoneme was evaluated by the angle of the line connecting the central pair (blue line, *Odf2*$^{+/+}$ cilia; red line, *Odf2*$^{\Delta Ex6,7/\Delta Ex6,7}$ cilia). This typical example was treated with 0.01% Triton X-100 to reveal the arrangements of the axonemes, but for the actual measurements we used untreated sections, shown in Figure S4D. The statistical analysis of rotational polarity is displayed in the circular plots bidirectionally. *Odf2*$^{+/+}$, n = 165; *Odf2*$^{\Delta Ex6,7/\Delta Ex6,7}$, n = 123. The black line was determined by the averaged orientation of the central pair in each thin-section image, which was set from 0° to ±180° axis. Scale bars, 0.2 μm.

(B) 3D reconstruction of the microtubule lattice. The image of the microtubules (green) was reconstructed and superimposed on single cross-sections. Scale bars, 0.2 μm.

(C) High-magnification image of a basal body/basal foot. Yellow arrows indicate microtubules. Note the tip of the basal foot is associated with microtubules. Scale bars, 0.1 μm.

See also Figure S6 and Movie S8.

Odf2 Deficiency Induces Concomitant Loss of the Apical Microtubular Lattice

Although basal feet, which indicate the polarity of *Odf2*$^{+/+}$ basal bodies (Gibbons, 1961; Reed et al., 1984), were not associated with *Odf2*$^{\Delta Ex6,7/\Delta Ex6,7}$ basal bodies, the polarization of *Odf2*$^{\Delta Ex6,7/\Delta Ex6,7}$ basal bodies might be determined by the polarization of shafts within the same cilia, due to their asymmetric 9+2 structure. Examination of the rotational polarity of the ciliary axonemes of *Odf2*$^{+/+}$ and *Odf2*$^{\Delta Ex6,7/\Delta Ex6,7}$ cilia revealed that *Odf2*$^{+/+}$ ciliary axonemes showed coordinated directionality but that the *Odf2*$^{\Delta Ex6,7/\Delta Ex6,7}$ ciliary axonemes did not (Figures 6A and S4D). Although the mutual relationship of the ciliary axonemes was partly coordinated in *Odf2*$^{\Delta Ex6,7/\Delta Ex6,7}$ cilia, possibly due to proximity effects (Guirao and Joanny, 2007; Guirao et al., 2010; Marshall, 2010; Mitchell et al., 2007), an overall statistical analysis illustrated by circular

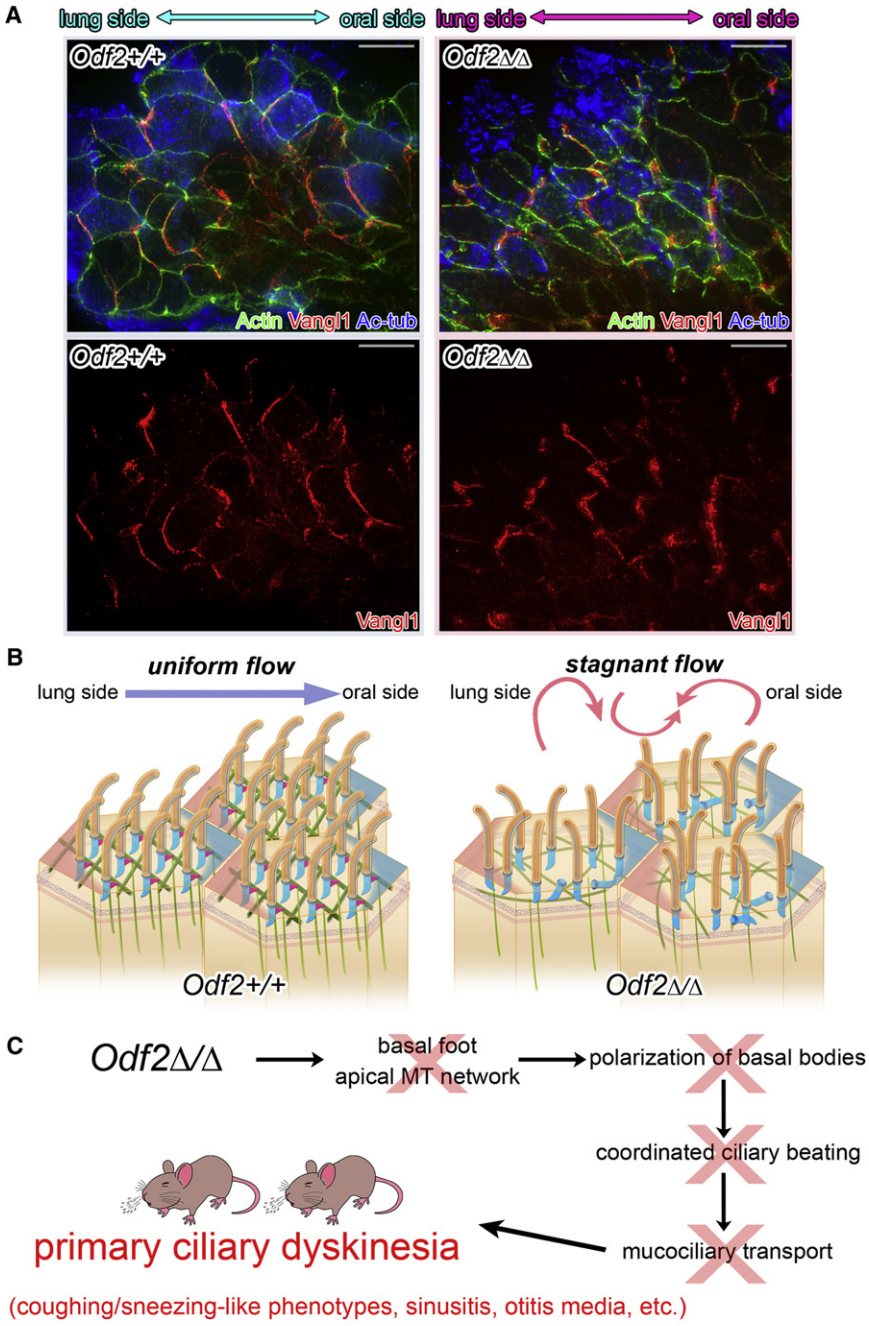

Figure 7. Asymmetric Distribution of PCP Core Protein Vangl 1, Schematic Illustrations of the Directionality of Ciliary Beating, and a Tentative Model for the *Odf2*$^{\Delta Ex6,7/\Delta Ex6,7}$ Phenotype

(A) Immunofluorescence staining showing the localization of Vangl 1, a PCP core protein, at the posterior side of tracheal cells in both the *Odf2*$^{+/+}$ and *Odf2*$^{\Delta Ex6,7/\Delta Ex6,7}$ mice. Actin, phalloidin (green); Vangl 1 (red); Ac-tub, acetylated α-tubulin (blue). Scale bars, 10 μm.

(B) Schematic illustrations of the basal bodies/feet and apical microtubular lattice in the ciliated epithelium. The anterior-posterior axis, determined by PCP, is indicated by the light-blue (anterior) and pink (posterior) coloring of the apical surface. Blue indicates basal bodies, pink illustrates basal feet, and green shows microtubules.

(C) Outline of the possible molecular events leading to the phenotypes of the *Odf2*$^{\Delta Ex6,7/\Delta Ex6,7}$ mice.

See also Figure S6.

plots indicated that rotational polarity was scattered (Figure 6A). We next asked whether the basal foot plays a role in the polarization of the basal body. Basal feet in *Odf2*$^{+/+}$, but not *Odf2*$^{\Delta Ex6,7/\Delta Ex6,7}$, tracheal epithelial cells associate with a regular array of apical microtubules (Figure 6B and Movie S8). This apical layer of microtubules was missing in *Odf2*$^{\Delta Ex6,7/\Delta Ex6,7}$ tissues. High-magnification imaging of *Odf2*$^{+/+}$ basal feet reveals that microtubules are attached to the tips of the basal feet (Figure 6C) (Anderson, 1972; Gordon, 1982; Reed et al., 1984).

It was recently suggested that actin filaments may play a role in the formation of multiciliary arrays in tracheal cells downstream of the dishevelled-related signaling pathway (Park et al., 2008). When we examined cortical actin by immunofluorescence, similar actin intensities were observed in *Odf2*$^{+/+}$ and *Odf2*$^{\Delta Ex6,7/\Delta Ex6,7}$ tracheal multiciliated cells (Figure S6A). We next processed the *Odf2*$^{+/+}$ and *Odf2*$^{\Delta Ex6,7/\Delta Ex6,7}$ tracheal multiciliated cells for thin-section electron microscopy in the presence or absence of heavy meromyosin (HMM) (Ishikawa et al., 1969; Reed et al., 1984). We found that there were no significant changes of cortical actin networks between the *Odf2*$^{+/+}$ and *Odf2*$^{\Delta Ex6,7/\Delta Ex6,7}$ tracheal multiciliated cells, consistent with the results of immunofluorescence imaging (Figure S6B). In *Odf2*$^{+/+}$ tracheal cells the actin filaments were occasionally associated with the basal feet, although the importance of this association remains unclear (Figure S6B). These findings point to the critical function of *Odf2*-based basal feet in the polarized organization of both the apical microtubular lattice and basal bodies, but not in the organization of the actin cortex (see the schematic drawing in Figure 7B).

Asymmetric Localization of Vangl 1 in Multiciliated Tracheal Cells Is Unaffected in *Odf2*$^{\Delta Ex6,7/\Delta Ex6,7}$ Mice

Because deficiency of full-length *Odf2* perturbed the PCP-dependent apical organization of microtubules, we tested whether the polarized distribution of PCP core proteins was

disturbed in these mice. To approach this question, we examined the specific localization of PCP core proteins, among which only the anti-Vangl 1 antibody was effective for immunofluorescence staining (Figure 7). To fix the direction of tracheal samples, we prepared the frozen sections in the longitudinal direction from the larynx to primary bronchi. In both *Odf2*$^{+/+}$ and *Odf2*$^{\Delta Ex6,7/\Delta Ex6,7}$ tracheal cells, Vangl 1 was highly enriched on the lung/posterior side, but not the oral/anterior side. The statistical analysis of distribution in the anterior-posterior direction indicated that the polarized distribution of PCP core proteins was not disturbed by deficiency of full-length *Odf2* (Figures 7A, 7B, and S6C).

DISCUSSION

We have shown that formation of basal feet requires *Odf2*, and plays a critical role in PCP-dependent multiciliary organization (Figures 7B and 7C). Since the first description of the basal foot in multiciliated cells by Gibbons (1961), it has been noted that the position of the basal foot generally indicates polarization of the basal bodies in multiciliated cells, although the molecular basis for this has remained unknown. Here, we have shown that the gene products of *Odf2*, Odf2/cenexin, are the essential structural components of the supramolecular complex that forms the basal foot. Because the deficiency of full-length *Odf2* resulted in loss of the entire basal foot structure from the basal body, *Odf2*$^{\Delta Ex6,7/\Delta Ex6,7}$ mice provide an ideal model system for the study of basal foot function.

The presence of primary cilia in *Odf2*$^{\Delta Ex6,7/\Delta Ex6,7}$ mice is in contrast with previous findings of loss of cilia phenotypes in *Odf2*$^{-/-}$ F9 cells. We discovered that 3′ terminal mRNA fragments of *Odf2* were expressed in *Odf2*$^{\Delta Ex6,7/\Delta Ex6,7}$ mice, but not expressed in *Odf2*$^{-/-}$ F9 cells. Furthermore, expression of the C-terminal region of Odf2/cenexin protein was detected in *Odf2*$^{\Delta Ex6,7/\Delta Ex6,7}$ tissues by immunofluorescence (Figure S1H). Expression of this C-terminal region of Odf2/cenexin appears to be sufficient for ciliogenesis because primary cilia were generated when a C-terminal construct of *Odf2* was introduced in *Odf2*$^{-/-}$ F9 cells (Figure 3D). Furthermore, a recent report also revealed that the C-terminal region of cenexin 1, one of the gene products of the *Odf2* gene, may be required for ciliogenesis in HeLa cells (Soung et al., 2009). Future work will examine more precisely how different regions of the Odf2 protein mediate ciliogenesis and basal foot formation.

The concurrent loss of basal feet and centrosomal subdistal appendages supports a molecular link between these two structures, although more detailed analysis will be required to unequivocally validate this analogy. The molecular mechanisms by which the centriolar subdistal appendages (which are evenly associated with all triplets of centrosomes) are transformed into basal feet (which are specifically associated with the 4,5,6-numbered triplets of basal bodies) will be of particular interest. In addition, the anchoring fiber and distal appendage show common characteristics. Both of these structures are associated with Odf2/cenexin, as shown by immunoelectron labeling (Figures 5C and S4A–S4C) (Nakagawa et al., 2001), and both remain in almost the same structures in *Odf2*$^{\Delta Ex6,7/\Delta Ex6,7}$ mice, with similar morphological characteristics (nine fine fibrous structures) as shown by UHVEMT (Figure S5 and Movie S7).

Our findings further support the idea that the basal foot is associated with a distinct part of the basal body, and plays a critical role in regulating polarization of the basal body under the control of PCP core proteins (Park et al., 2008; Vladar and Axelrod, 2008; Wallingford, 2010). It is worth considering possible roles of the association of basal bodies with cytoplasmic microtubules through basal feet. In contrast to the well-developed microtubular lattice in *Odf2*$^{+/+}$ multiciliated cells, this structure disappeared upon deletion of exon 6 and 7 of *Odf2*, suggesting a critical role for direct or indirect association between basal feet and microtubules. Thin-section electron microscopy and UHVEMT revealed that *Odf2*$^{+/+}$ basal feet are associated with microtubules at the tips of basal feet, consistent with previous observations (Reed et al., 1984). Given that immunoelectron microscopic labeling for Odf2/cenexin indicated that they were preferably associated with the basal feet near the border between basal feet and basal bodies, it appears most likely that some basal foot components other than Odf2/cenexin bind directly to microtubules at the tips of basal feet. The association between basal feet and microtubules was partly supported by the immunoelectron microscopic images using an anti-γ-tubulin antibody (data not shown), consistent with a previous report in which γ-tubulin was associated with the basal feet (Hagiwara et al., 2000). Thus, the interaction between basal feet and microtubules plays a key role in formation of microtubular lattice just below the apical membrane in multiciliated cells, providing a possible insight into how PCP cues, under the control of PCP core proteins, lead to the polarized arrangement of basal bodies (Jones et al., 2008).

The docking of basal bodies to the apical membranes was previously shown to be affected by defects in actin organization in *dishevelled*-KD *Xenopus* multiciliated cells (Park et al., 2006, 2008). In the present study it was found that actin filaments were associated similarly with *Odf2*$^{+/+}$ and *Odf2*$^{\Delta Ex6,7/\Delta Ex6,7}$ basal bodies, suggesting that Odf2/cenexin seemingly function downstream or independent (but not upstream) of *dishevelled*-dependent regulation of actin organization. It is likely that the loss of the interaction between basal feet and microtubules in *Odf2*$^{\Delta Ex6,7/\Delta Ex6,7}$ basal bodies may cause a partial defect in the transport and/or docking of *Odf2*$^{\Delta Ex6,7/\Delta Ex6,7}$ basal bodies to the apical membrane.

Our observation that basal body polarization is disrupted despite normal localization of PCP core proteins in *Odf2*$^{\Delta Ex6,7/\Delta Ex6,7}$ tracheal multiciliated cells suggests that the arrangement of basal bodies is specifically downstream of and/or independent of asymmetric localization of PCP core proteins and that Odf2/cenexin may play a role as PCP effectors. In cells in which PCP core proteins such as Dishevelled (Park et al., 2008) and/or Vangl species (Guirao et al., 2010) were knocked down, basal feet remain associated with basal bodies, the polarization of which is disturbed. A similar phenotype, in which basal body alignment is disrupted but basal feet persist, is observed in various mouse models of primary ciliary dyskinesia. It seems likely that Odf2/cenexin function in response to a specific branch of the PCP effector network, and

further work will be required to characterize the precise relationship between basal feet and PCP signaling.

In the present study, taking advantage of the *Odf2*$^{\Delta Ex6,7/\Delta Ex6,7}$ mouse model, we have revealed the critical function of *Odf2* in the formation of basal feet, the role of these structures in the polarization of basal bodies, and their requirement for the coordinated beating of cilia. Further analysis of the components of basal feet will lead to a better understanding of the regulation of polarization of basal bodies, and *Odf2*$^{\Delta Ex6,7/\Delta Ex6,7}$ mice will provide an excellent model system for future studies.

EXPERIMENTAL PROCEDURES

Generation of *Odf2*$^{\Delta Ex6,7/\Delta Ex6,7}$ Mice

The targeting cassette consisted of floxed exons 6 and 7 of *Odf2* in tandem with the neomycin-resistance gene in intron 5, flanked by another *loxP* site (Figure 1). All animal experiments were performed with the approval of the institutional animal care and use committee at the University of Osaka.

Quantitative Real-Time RT-PCR

Quantitative real-time RT-PCR analysis was performed as described previously (Kunimoto et al., 2009), using the primers for the C-terminal region of *Odf2*: (5′ primer) GCTGAAGGCGTCAGTGAAGAACTAC, (3′ primer) CTCTAGC TGTGCAGCCACTTCATC.

Analysis of Respiratory Sounds

To analyze the respiratory sounds of the mice, we used the free speech analysis software Praat (Version 5.1.22) (for details, see Extended Experimental Procedures).

Antibodies

To detect Odf2/cenexin in immunofluorescence, we used three rabbit polyclonal antibodies, Odf2-N1 pAb (HPA001874; Sigma-Aldrich) and Odf2-N2 pAb (characterized previously by Ishikawa et al., 2005), and rabbit anti-Odf2/cenexin pAb (ab43840; Abcam), which recognizes the C-terminal region of Odf2/cenexin. For immunoblotting, Odf2-N1 and -N2 pAbs were used. Rabbit anti-mouse ninein pAb was characterized previously (Ishikawa et al., 2005). Rabbit anti-γ-tubulin pAb (T3559; Sigma-Aldrich), mouse anti-acetylated-α-tubulin monoclonal antibody (6-11B-1) (T6793; Sigma-Aldrich), Rabbit anti-human Vangl 1 pAb (HPA025235; Sigma-Aldrich), and rabbit anti-mouse GAPDH pAb (G9545; Sigma-Aldrich) were obtained from commercial sources.

Immunofluorescence Microscopy

After the samples were processed as described previously (Kunimoto et al., 2009), they were observed using a DeltaVision microscope (Applied Precision, Issaquah, WA, USA). For immunostaining by Odf2-N1 and -N2 pAbs, citraconic anhydrate (Immunosaver; Nissin EM, Tokyo) was used for antigen retrieval according to the manufacturer's instructions.

Scanning Electron Microscopy

The trachea was isolated and processed conventionally for scanning electron microscopy. Observations were performed on an S-4800 scanning electron microscope (Hitachi).

Visualization of Ciliary Beating and Mucociliary Transport

Mouse tracheal movements and the flow of fluorescent beads were recorded by a high-speed video camera (HAS-200, Detect) connected to an Axiophot microscope (Zeiss) and by a CSU-X confocal unit (Yokogawa) and an iXon EMCCD camera (Andor Technology) connected to a DMI6000B microscope (Leica), respectively (for details, see Extended Experimental Procedures).

Electron Microscopy

For thin-section electron microscopy, mouse tracheas, with or without HMM decoration, were processed according to the classical method (Ishikawa et al., 1969). For immunolabeling of Odf2/cenexin and γ-tubulin, Odf2-N2 pAb or rabbit anti-γ-tubulin pAb (T3559; Sigma-Aldrich) was used (for details, see Extended Experimental Procedures).

Electron Tomography with Ultra-High-Voltage Electron Microscopy

For observation by UHVEMT, 700 nm thick sections were cut and observed in an ultra-high-voltage electron microscope operating at 1–2 MeV (H-3000; Hitachi). The images were taken at 25,000× from −60° to +60° at 2° intervals around a single axis tilt series (for details, see Extended Experimental Procedures).

SUPPLEMENTAL INFORMATION

Supplemental Information includes Extended Experimental Procedures, six figures, and eight movies and can be found with this article online at doi:10.1016/j.cell.2011.10.052.

ACKNOWLEDGMENTS

We are grateful to Y. Fujiyoshi, S. Kitajiri, T. Stearns, A. Wynshaw-Boris, and our laboratory members for discussion. We thank D. Sipp for critical reading of this manuscript. We thank Shu Lin Low, S. Watanabe, and R. Tokumasu for limited experimental collaboration. We thank M. Uji and A. Hagiwara for the excellent technical assistance. We also thank Y. Ohta, H. Mori, A. Takaoka, S. Yoshiba, K. Takaoka, I. Tateya, H. Shiratori, M. Inagaki, A. Inoko, and M. Ibi for technical advice. This work was supported in part by Grants-in-Aid for Creative Scientific Research (to Sachiko Tsukita) and Global COE Program (Integrative Life Science Based on the Study of Biosignaling Mechanisms) from the Ministry of Education, Culture, Sports, Science, and Technology of Japan. This work is dedicated to Shoichiro Tsukita, who contributed the initial planning of this study and passed away in 2005. Research planning and supervision were by Sachiko Tsukita and K.K. All experiments were conducted by K.K. in collaboration with H.I. (instruction in construction of targeting vector), Y.Y. (western blotting and RT-PCR), K.S./H.H. (live imaging), T. Nishida/T.H. (UHVEMT), A.T./T. Noda (generation of knockout mice), and H.I. and Y.Y. (transfection of F9 cells). Discussion was by K.K., Y.Y., K.S., T. Nishida, H.H., H.I., T.O., A.T, T. Noda, and Sachiko Tsukita. Discussion and manuscript writing were mainly by Sachiko Tsukita, K.K., and Y.Y.

Received: February 2, 2011
Revised: June 15, 2011
Accepted: October 31, 2011
Published: January 19, 2012

REFERENCES

Afzelius, B.A. (1979). The immotile-cilia syndrome and other ciliary diseases. Int. Rev. Exp. Pathol. *19*, 1–43.

Anderson, R.G. (1972). The three-dimensional structure of the basal body from the rhesus monkey oviduct. J. Cell Biol. *54*, 246–265.

Badano, J.L., Mitsuma, N., Beales, P.L., and Katsanis, N. (2006). The ciliopathies: an emerging class of human genetic disorders. Annu. Rev. Genomics Hum. Genet. *7*, 125–148.

Boisvieux-Ulrich, E., Laine, M.C., and Sandoz, D. (1985). The orientation of ciliary basal bodies in quail oviduct is related to the ciliary beating cycle commencement. Biol. Cell *55*, 147–150.

Bornens, M. (2002). Centrosome composition and microtubule anchoring mechanisms. Curr. Opin. Cell Biol. *14*, 25–34.

Brohmann, H., Pinnecke, S., and Hoyer-Fender, S. (1997). Identification and characterization of new cDNAs encoding outer dense fiber proteins of rat sperm. J. Biol. Chem. *272*, 10327–10332.

Gibbons, I.R. (1961). The relationship between the fine structure and direction of beat in gill cilia of a lamellibranch mollusc. J. Biophys. Biochem. Cytol. *11*, 179–205.

Gordon, R.E. (1982). Three-dimensional organization of microtubules and microfilaments of the basal body apparatus of ciliated respiratory epithelium. Cell Motil. *2*, 385–391.

Gray, R.S., Abitua, P.B., Wlodarczyk, B.J., Szabo-Rogers, H.L., Blanchard, O., Lee, I., Weiss, G.S., Liu, K.J., Marcotte, E.M., Wallingford, J.B., and Finnell, R.H. (2009). The planar cell polarity effector Fuz is essential for targeted membrane trafficking, ciliogenesis and mouse embryonic development. Nat. Cell Biol. *11*, 1225–1232.

Guirao, B., and Joanny, J.F. (2007). Spontaneous creation of macroscopic flow and metachronal waves in an array of cilia. Biophys. J. *92*, 1900–1917.

Guirao, B., Meunier, A., Mortaud, S., Aguilar, A., Corsi, J.M., Strehl, L., Hirota, Y., Desoeuvre, A., Boutin, C., Han, Y.G., et al. (2010). Coupling between hydrodynamic forces and planar cell polarity orients mammalian motile cilia. Nat. Cell Biol. *12*, 341–350.

Hagiwara, H., Kano, A., Aoki, T., Ohwada, N., and Takata, K. (2000). Localization of gamma-tubulin to the basal foot associated with the basal body extending a cilium. Histochem. J. *32*, 669–671.

Hard, R., and Rieder, C.L. (1983). Muciliary transport in newt lungs: the ultrastructure of the ciliary apparatus in isolated epithelial sheets and in functional triton-extracted models. Tissue Cell *15*, 227–243.

Heydeck, W., Zeng, H., and Liu, A. (2009). Planar cell polarity effector gene Fuzzy regulates cilia formation and Hedgehog signal transduction in mouse. Dev. Dyn. *238*, 3035–3042.

Ishikawa, H., Bischoff, R., and Holtzer, H. (1969). Formation of arrowhead complexes with heavy meromyosin in a variety of cell types. J. Cell Biol. *43*, 312–328.

Ishikawa, H., Kubo, A., Tsukita, S., and Tsukita, S. (2005). Odf2-deficient mother centrioles lack distal/subdistal appendages and the ability to generate primary cilia. Nat. Cell Biol. *7*, 517–524.

Jones, C., Roper, V.C., Foucher, I., Qian, D., Banizs, B., Petit, C., Yoder, B.K., and Chen, P. (2008). Ciliary proteins link basal body polarization to planar cell polarity regulation. Nat. Genet. *40*, 69–77.

Kunimoto, K., Nojima, H., Yamazaki, Y., Yoshikawa, T., Okanoue, T., and Tsukita, S. (2009). Involvement of IQGAP3, a regulator of Ras/ERK-related cascade, in hepatocyte proliferation in mouse liver regeneration and development. J. Cell. Physiol. *220*, 621–631.

Lange, B.M., and Gull, K. (1995). A molecular marker for centriole maturation in the mammalian cell cycle. J. Cell Biol. *130*, 919–927.

Lüders, J., and Stearns, T. (2007). Microtubule-organizing centres: a re-evaluation. Nat. Rev. Mol. Cell Biol. *8*, 161–167.

Marshall, W.F. (2010). Cilia self-organize in response to planar cell polarity and flow. Nat. Cell Biol. *12*, 314–315.

Marshall, W.F., and Kintner, C. (2008). Cilia orientation and the fluid mechanics of development. Curr. Opin. Cell Biol. *20*, 48–52.

McNeill, H. (2010). Planar cell polarity: keeping hairs straight is not so simple. Cold Spring Harb. Perspect. Biol. *2*, a003376.

Mitchell, B., Jacobs, R., Li, J., Chien, S., and Kintner, C. (2007). A positive feedback mechanism governs the polarity and motion of motile cilia. Nature *447*, 97–101.

Morillas, H.N., Zariwala, M., and Knowles, M.R. (2007). Genetic causes of bronchiectasis: primary ciliary dyskinesia. Respiration *74*, 252–263.

Nakagawa, Y., Yamane, Y., Okanoue, T., Tsukita, S., and Tsukita, S. (2001). Outer dense fiber 2 is a widespread centrosome scaffold component preferentially associated with mother centrioles: its identification from isolated centrosomes. Mol. Biol. Cell *12*, 1687–1697.

Oko, R., and Clermont, Y. (1988). Isolation, structure and protein composition of the perforatorium of rat spermatozoa. Biol. Reprod. *39*, 673–687.

Park, T.J., Haigo, S.L., and Wallingford, J.B. (2006). Ciliogenesis defects in embryos lacking inturned or fuzzy function are associated with failure of planar cell polarity and Hedgehog signaling. Nat. Genet. *38*, 303–311.

Park, T.J., Mitchell, B.J., Abitua, P.B., Kintner, C., and Wallingford, J.B. (2008). Dishevelled controls apical docking and planar polarization of basal bodies in ciliated epithelial cells. Nat. Genet. *40*, 871–879.

Reed, W., Avolio, J., and Satir, P. (1984). The cytoskeleton of the apical border of the lateral cells of freshwater mussel gill: structural integration of microtubule and actin filament-based organelles. J. Cell Sci. *68*, 1–33.

Schweizer, S., and Hoyer-Fender, S. (2009). Mouse Odf2 localizes to centrosomes and basal bodies in adult tissues and to the photoreceptor primary cilium. Cell Tissue Res. *338*, 295–301.

Seeley, E.S., and Nachury, M.V. (2010). The perennial organelle: assembly and disassembly of the primary cilium. J. Cell Sci. *123*, 511–518.

Sloboda, R.D., and Rosenbaum, J.L. (2007). Making sense of cilia and flagella. J. Cell Biol. *179*, 575–582.

Sorokin, S.P. (1968). Reconstructions of centriole formation and ciliogenesis in mammalian lungs. J. Cell Sci. *3*, 207–230.

Soung, N.K., Kang, Y.H., Kim, K., Kamijo, K., Yoon, H., Seong, Y.S., Kuo, Y.L., Miki, T., Kim, S.R., Kuriyama, R., et al. (2006). Requirement of hCenexin for proper mitotic functions of polo-like kinase 1 at the centrosomes. Mol. Cell. Biol. *26*, 8316–8335.

Soung, N.K., Park, J.E., Yu, L.R., Lee, K.H., Lee, J.M., Bang, J.K., Veenstra, T.D., Rhee, K., and Lee, K.S. (2009). Plk1-dependent and -independent roles of an ODF2 splice variant, hCenexin1, at the centrosome of somatic cells. Dev. Cell *16*, 539–550.

Sternberg, N., Hamilton, D., and Hoess, R. (1981). Bacteriophage P1 site-specific recombination. II. Recombination between loxP and the bacterial chromosome. J. Mol. Biol. *150*, 487–507.

Tarnasky, H., Cheng, M., Ou, Y., Thundathil, J.C., Oko, R., and van der Hoorn, F.A. (2010). Gene trap mutation of murine outer dense fiber protein-2 gene can result in sperm tail abnormalities in mice with high percentage chimaerism. BMC Dev. Biol. *10*, 67.

Vladar, E.K., and Stearns, T. (2007). Molecular characterization of centriole assembly in ciliated epithelial cells. J. Cell Biol. *178*, 31–42.

Vladar, E.K., and Axelrod, J.D. (2008). Dishevelled links basal body docking and orientation in ciliated epithelial cells. Trends Cell Biol. *18*, 517–520.

Voronina, V.A., Takemaru, K., Treuting, P., Love, D., Grubb, B.R., Hajjar, A.M., Adams, A., Li, F.Q., and Moon, R.T. (2009). Inactivation of Chibby affects function of motile airway cilia. J. Cell Biol. *185*, 225–233.

Wallingford, J.B. (2010). Planar cell polarity signaling, cilia and polarized ciliary beating. Curr. Opin. Cell Biol. *22*, 597–604.

Zallen, J.A. (2007). Planar polarity and tissue morphogenesis. Cell *129*, 1051–1063.

Zariwala, M.A., Knowles, M.R., and Omran, H. (2007). Genetic defects in ciliary structure and function. Annu. Rev. Physiol. *69*, 423–450.